340
4/23/80
30

DR. 1132

DOE/ET/23011-T1

BORON ARSENIDE THIN FILM SOLAR CELL DEVELOPMENT

Quarterly Report No. 1

By
Jack L. Boone
Thomas P. Van Doren

MASTER

July 1979

Work Performed Under Contract No. AC04-79ET23011

Eagle-Picher Industries, Inc.
Miami Research Laboratories
Miami, Oklahoma

U.S. Department of Energy

Solar Energy

DISCLAIMER

This report was prepared as an account of work sponsored by an agency of the United States Government. Neither the United States Government nor any agency Thereof, nor any of their employees, makes any warranty, express or implied, or assumes any legal liability or responsibility for the accuracy, completeness, or usefulness of any information, apparatus, product, or process disclosed, or represents that its use would not infringe privately owned rights. Reference herein to any specific commercial product, process, or service by trade name, trademark, manufacturer, or otherwise does not necessarily constitute or imply its endorsement, recommendation, or favoring by the United States Government or any agency thereof. The views and opinions of authors expressed herein do not necessarily state or reflect those of the United States Government or any agency thereof.

DISCLAIMER

Portions of this document may be illegible in electronic image products. Images are produced from the best available original document.

DISCLAIMER

"This book was prepared as an account of work sponsored by an agency of the United States Government. Neither the United States Government nor any agency thereof, nor any of their employees, makes any warranty, express or implied, or assumes any legal liability or responsibility for the accuracy, completeness, or usefulness of any information, apparatus, product, or process disclosed, or represents that its use would not infringe privately owned rights. Reference herein to any specific commercial product, process, or service by trade name, trademark, manufacturer, or otherwise, does not necessarily constitute or imply its endorsement, recommendation, or favoring by the United States Government or any agency thereof. The views and opinions of authors expressed herein do not necessarily state or reflect those of the United States Government or any agency thereof."

This report has been reproduced directly from the best available copy.

Available from the National Technical Information Service, U. S. Department of Commerce, Springfield, Virginia 22161.

Price: Paper Copy $7.00
Microfiche $3.50

DOE/ET/23011-T1
Distribution Category UC-63e

BORON ARSENIDE THIN FILM SOLAR CELL DEVELOPMENT

Paul E. Grayson, Program Manager
Gene Cantwell, Project Engineer

Miami Research Laboratories
Eagle-Picher Industries, Inc.
Miami, Oklahoma 74354

CO-AUTHORS: Jack L. Boone, UMR
Thomas P. Van Doren, UMR

QUARTERLY REPORT #1

JULY 1979

PREPARED UNDER CONTRACT NO. DE-AC04-79ET23011

FOR

SOLAR ENERGY RESEARCH INSTITUTE
PHOTOVOLTAIC PROGRAM OFFICE
Golden, Colorado

ACKNOWLEDGEMENT

The authors wish to acknowledge the assistance of Mr. Tom Potts for the design and construction of the gas handling system and the safety system, Mr. Joe Powderly for assistance in substrate preparation, and Ms. Janice Black for equipment preparation and assistance with depositions.

ABSTRACT

This document is a report on the Eagle-Picher Industries, Inc. Boron Arsenide Contract with D.O.E. (No. DE-AC04-79ET23011). This contract was initiated on April 9, 1979 and is presently funded for one year.

A large portion of the effort expended in the first quarter was devoted to the design, assembly, and testing of the film growth apparatus. The reactor has been completed and tested by depositing boron from diborane gas onto heated quartz substrates. The objective of this effort was to achieve film growth, which has been accomplished. Within the last month, attempts to grow boron arsenide films have been made by introducing both diborane and arsine into the reactor. Thin films have been grown on quartz and sapphire (alumina) substrates. Variations in film thickness, composition, degree of crystallinity, and conductivity have been observed as a result of variation of the deposition parameters, such as type and flow rate of carrier gases, substrate temperature, and substrate materials. X-ray analysis of several samples indicates that films containing boron and arsenic have been grown. No crystalline films have been produced to date.

Electrical and optical measurements by the University of Missouri-Rolla (UMR) subcontractor indicates some correlation between at least one of the films grown and the results achieved by Chu, et al. on BAs. Thus far, the electrical conductivity, film topography, optical absorption, index of refraction, impurity type, and photo-conductivity have been investigated on one sample. This material appears to be B_xAs_y and could

be BAs. Further investigations will be required to be conclusive.

During the next quarter, the primary objectives are to:

(1) optimize deposition parameters,

(2) make conductivity and Hall measurements on a larger number and variety of samples,

(3) make photoconductivity measurements and,

(4) study the film growth mechanisms in much more detail.

TABLE OF CONTENTS

Section		Page
	ABSTRACT	i
	LIST OF FIGURES	iv
	LIST OF TABLES	v
	INTRODUCTION	
1.	DESIGN AND CONSTRUCTION OF THE DIBORANE-ARSINE REACTOR	3
	1.1 THE DEPOSITION REACTOR	3
	1.2 THE GAS HANDLING SYSTEM	8
	1.3 THE SAFETY SYSTEM	10
	1.4 CALIBRATION OF THE DEPOSITION SYSTEM	12
2.	FILM GROWTH	14
	2.1 DIBORANE DEPOSITIONS	14
	2.2 DIBORANE - ARSINE DEPOSITIONS	20
3.	OPTICAL AND ELECTRICAL MEASUREMENTS	30
	3.1 OPTICAL MEASUREMENTS	30
	3.2 ELECTRICAL CONDUCTIVITY MEASUREMENTS	39
	3.3 LIFETIME MEASUREMENT AND LIGHT SCANNING SYSTEMS	46
4.	WORK PLANNED FOR NEXT QUARTER	47
	4.1 FILM GROWTH	47
	4.2 OPTICAL AND ELECTRICAL MEASUREMENTS	48

LIST OF FIGURES

Figures

1. Deposition Reactor 4
2. Grafoil Heater Strip 5
3. Deposition Reactor with Grafoil Heater Strip in Place 7
4. Deposition Reactor with Substrate and Mask in Place 7
5. Gas Handling System 9
6. Walk-In Hood Containing the Gases and Gas Handling System 11
7. Walk-In Hood Containing the Deposition Reactor 11
8. SEM Photograph of Boron Deposition #1. 2500X 18
9. SEM Photograph of Boron Deposition #1. 200X 18
10. SEM Photograph of Edge of Film #11. 5000X 26
11. SEM Photograph of Surface of Film #11. 30,000X 26
12. SEM Photograph of Edge of Film #13. 1500X 27
13. SEM Photograph of Surface of Film #13. 30,000X 27
14. Infrared Transmission Data for Sample #11 on a Sapphire Substrate. 31
15. Infrared Transmission Data for Sample #13 on a Sapphire Substrate. 32
16. Absorbance Versus Wavelength Over the Visible Spectrum for Sample #11. 33
17. Absorbance Versus Wavelength Over the Visible Spectrum for Sample #13. 34
18. Absorption Coefficient vs. Incident Photon Energy for Films #11 and #13. 36
19. $(\alpha \ell)^2$ vs. Incident Photon Energy for Films #11 and #13. 37
20. $(\alpha \ell)^{0.5}$ vs. Incident Photon Energy for Films #11 and #13. 38
21. Log σ vs. 1/T for the Low Temperature Range. Sample #11. 42
22. Log σ vs. 1/T for the High Temperature Range. Sample #11. 43

LIST OF TABLES

Table		Page
I	Diborane Deposition Parameters and Results.	16
II	Substrate Preparation Techniques for Diborane Depositions.	19
III	Substrate Preparation Techniques for Diborane Arsine Depositions.	22
IV	Diborane Arsine Deposition Parameters and Results Using Argon as the Carrier Gas.	23
V	Diborane Arsine Deposition Parameters and Results Using Hydrogen as the Carrier Gas	28
VI	Room Temperature Conductivity for Films #11 and #13.	40

INTRODUCTION

This first quarterly report covers the work performed on United States Department of Energy contract number DE-AC04-79ET23011 by the Miami Research Laboratories (MRL) of Eagle-Picher Industries, Inc. and its subcontractor, the Electrical Engineering Department of the University of Missouri-Rolla, during the period from April 9, 1979 to July 9, 1979. The program goal is to evaluate thin film polycrystalline boron arsenide (BAs) as a photovoltaic material. The first year's effort will emphasize the growth and characterization of bulk films and the second year's work will evaluate junction formation and solar cell performance.

BAs is a III-V semiconducting compound with a direct energy gap of 1.46 eV and an associated limit conversion efficiency of 24% under AM1 conditions. It has a cubic structure with a lattice parameter of 4.777Å. The large optical absorption coefficient, nearly total covalent bonding, and the abundance of the elements boron and arsenic provide additional motivation for a thorough evaluation of BAs.

The Miami Research Laboratories (MRL) is the prime contractor and provides overall project management. The film growth, and physical and chemical characterization are also the responsibilities of MRL. Metal contacting, electrical measurements, and solar cell performance evaluation are the responsibilities of the University of Missouri-Rolla (UMR).

During the first quarter, the following major work tasks were performed:

1. The diborane (B_2H_6) and arsine (AsH_3) reactor was designed, assembled, and tested. A special emphasis was placed on safety engineering because of the toxicity of the compounds involved.

2. Seven films were grown initially using only B_2H_6 and Ar in order to confirm safe operation of the reactor. Eleven films were grown using B_2H_6 and AsH_3 with either Ar or H_2 as a carrier gas.

3. X-ray, SEM, optical, and electrical characterization was initiated on the majority of these films. The results on two films are nearly complete, and are included in this report.

1. DESIGN AND CONSTRUCTION OF THE DIBORANE-ARSINE REACTOR

1.1 THE DEPOSITION REACTOR

Accurate temperature control and reproducibility were prime concerns in the design of the deposition reactor. These criteria are important because of the very narrow range of expected deposition temperatures: BAs decomposes to $B_{13}As_2$ at temperatures greater than 920^oC and the expected growth temperatures are above 800^oC. Another criterion is that the reactor should be cold walled to help suppress gas-phase nucleation.

To achieve accurate temperature control, an automatic temperature controller with a thermocouple input seemed most promising. This indicated that resistance heating as opposed to induction heating should be used to avoid any problems of RF interference with the temperature control circuit. The condition that the walls of the reactor be kept cold to suppress gas-phase nucleation indicated that it would be necessary to design a special reactor for this deposition.

The reactor design selected was a vertical downward flow chamber with a flexible graphite (Grafoil[1]) heating strip and with water-cooled feed throughs to supply the power. A cross-sectional view of this reactor is shown in Figure 1. Although several other heater materials were considered, the Grafoil was used because of its low cost and low thermal coefficient of expansion. In addition grafoil can be easily cut to a desired configuration to alter the heated zone and thus give uniform temperatures across the face of the heated substrate. After trying several con-

[1] Registered trademark of Union Carbide Corporation.

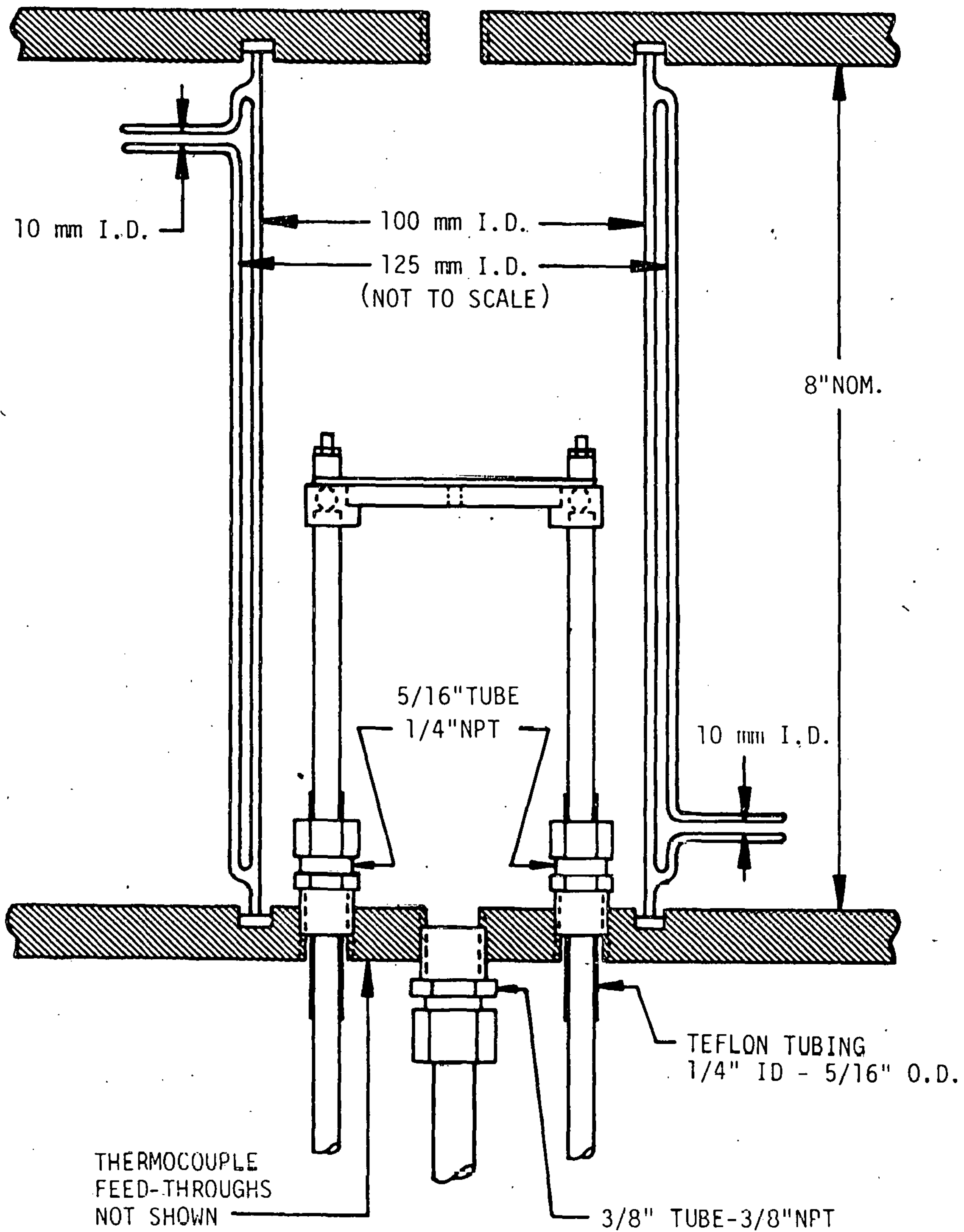

Figure 1. Deposition Reactor.

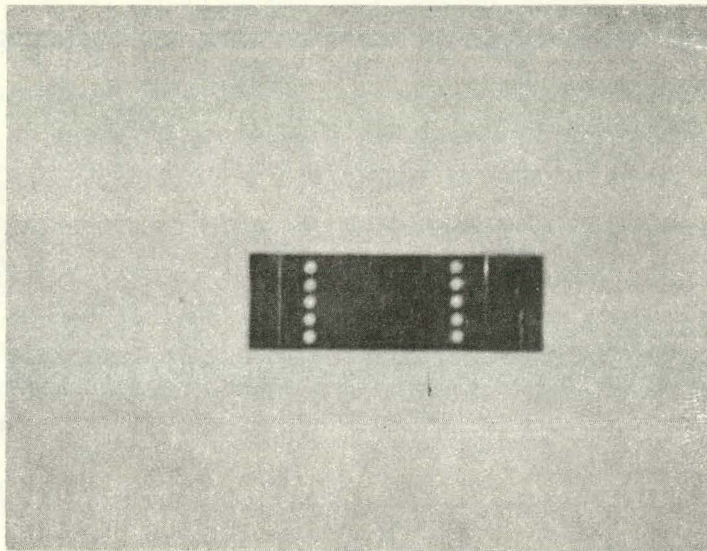

Figure 2. Grafoil Heater Strip.

figurations, it was found that a 1" by 2" by 10 mil thick strip of Grafoil shaped in the configuration shown in Figure 2 gave reproducible uniform temperatures (less than 10^{0}C variation) on a .035" thick silicon substrate. These measurements were made with argon as the carrier gas. The temperature distribution when using hydrogen as the carrier has not been measured at this time. The water-cooled copper electrodes consist of 1/4" copper tubing with machined, brass fixtures (drilled for coolant water transfer) for clamping the Grafoil heater strip. Each feed through post is electrically insulated from the bottom of the reactor by a 5/16" O.D. sleeve of teflon. The seal between the bottom of the reactor and the feed through is formed by the swaging action of the standard thermocouple feed through fittings attached to the bottom of the reactor. A 1/4" thick by 1" wide by 2" long plate of hot pressed boron nitride is placed between the posts directly beneath the Grafoil-strip to support the flexible heater strip, separate the electrodes by the proper distance, and act as a fixture for the controlling thermocouple. This thermocouple is embedded in the top of the boron nitride plate next to, but not touching, the Grafoil heating strip. The thermocouple passes through the bottom of the reactor, epoxied into a 1/8" 316 - stainless steel tube. The seal between this tube and the bottom of the reactor is also made by the swaging action of a thermocouple feed through fitting. A photograph of this assembly is shown in Figure 3. The thermocouple is connected to the temperature controller and a digital thermometer, which gives the temperature when the controller is bypassed and the power is controlled manually.

The substrate is placed in the center of the heater. The largest size substrate that has been used is 1/2" X 3/4". An accurately machined

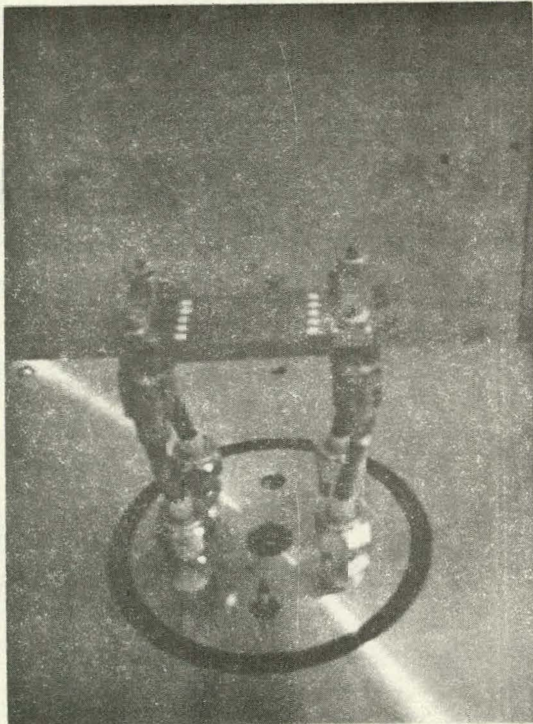

Figure 3. Deposition Reactor with Grafoil Heater Strip in Place.

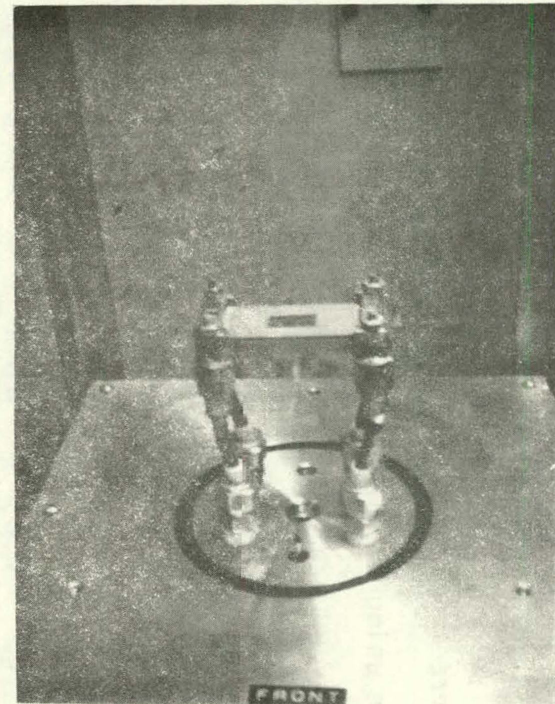

Figure 4. Deposition Reactor with Substrate and Mask in Place.

mask of the same thickness surrounds the substrate to hold it in place and promote a uniform temperature across the face of the substrate. Boron nitride was initially tried as the material for this mask but it was found that Lavite (or Grade A lava) was a preferable material since it promoted a more uniform temperature on the surface of the substrate. Figure 4 shows the apparatus with the substrate and mask in place.

The sides of the reactor are double-walled quartz tubing with provisions for water cooling. These seat against neoprene seals riding in machined grooves in the 316 stainless steel reactor end plates. These end plates are also drilled and tapped for the thermocouple and power feed throughs, and the gas inlet and outlet. The gas inlet and outlet are situated along the vertical, center axis of the reactor.

1.2 THE GAS HANDLING SYSTEM

The gas handling system was designed with both safety and purity in mind. A diagram of the system is given in Figure 5. The construction material is entirely 316 stainless steel. Properly sized flow meters measure the flow of reactant, carrier, and etchant gases. Electrically actuated, normally closed solenoid valves are used immediately after the diborane and arsine regulators to automatically shut off these flows in the event of an emergency. Either hydrogen or argon can be used as the carrier gas and helium can be admitted to the system to allow leak-checking the system with a sensitive electronic leak detector. Two vacuum pumps are attached to the system. One pump is used to vacuum purge the diborane and arsine regulators prior to opening the tank

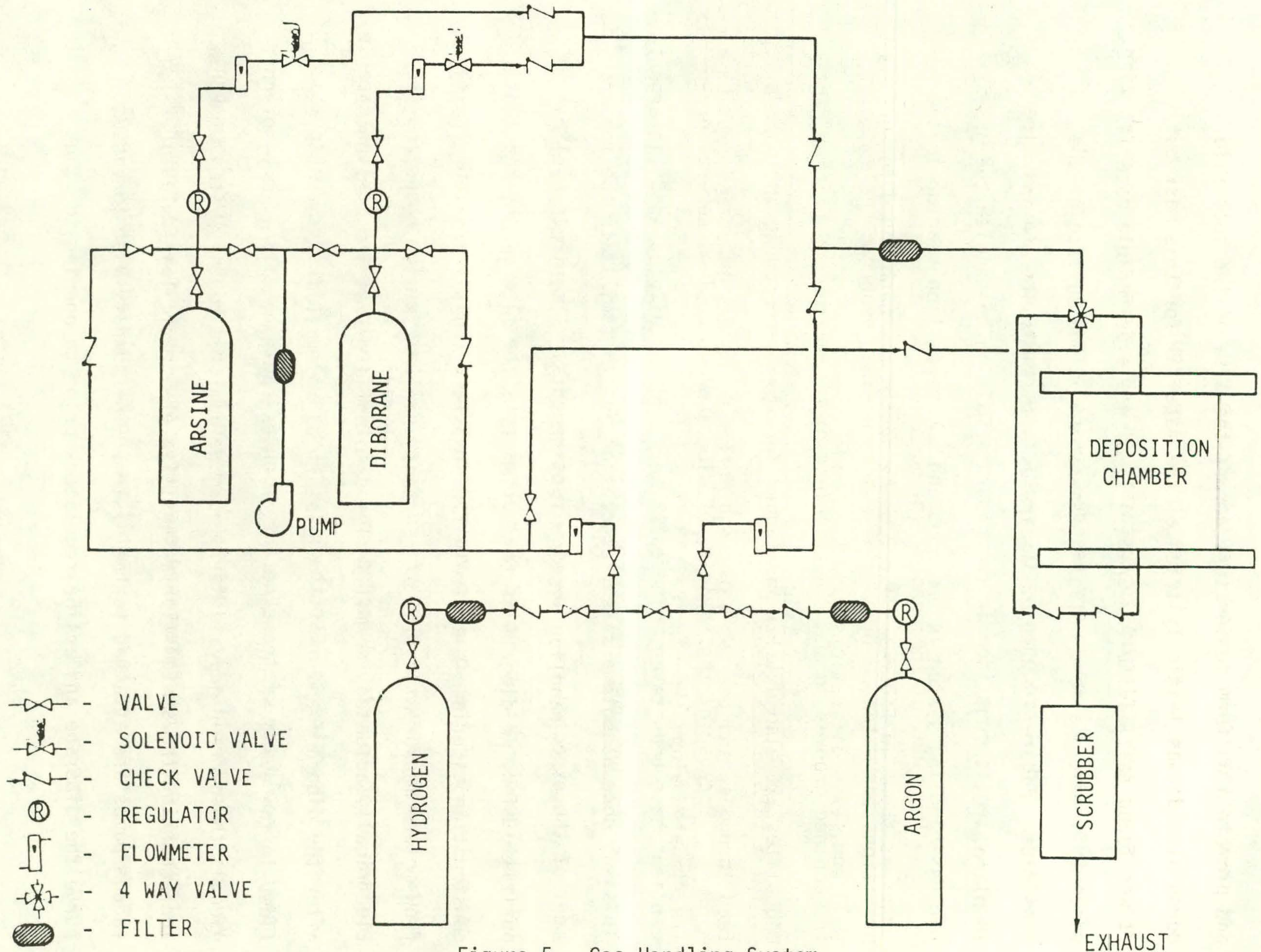

Figure 5. Gas Handling System.

valves and to remove any residual impurities or toxic gases after closing the tank valves. The second pump is used to vacuum purge the entire system, exclusive of the diborane and arsine regulators, to reduce the moisture and contaminants contained in the system prior to deposition. It is also used to remove any residual gases from the reactor after deposition and before opening the reactor to remove the sample. The whole system is contained in two separate walk-in hoods with the gases and gas-handling system in one hood and the deposition reactor in the other as shown in Figures 6 and 7. The design has been found to work well and few modifications have been made.

1.3 THE SAFETY SYSTEM

Because of the toxicity of diborane and arsine, several precautions have been taken. The gases were ordered diluted to 5% in argon. This was done as both a safety precaution and to facilitate the measurement of the expected very low flow requirements. A control panel has been designed and constructed that interlocks the flow of the reactant gases (by way of the solenoid valves) to several safety related requirements; such as adequate pressure differential between the hoods and the working area, and closed hood doors. An electronic arsine monitor capable of detecting arsine to less than 0.05 ppm is also interlocked into this panel. Should any of these detect an undesirable condition, the solenoid valves are automatically closed and an audible alarm is sounded. A panic button for operation determined emergency shut down is also provided. Emergency procedures have been written and correlated with the local hospital emergency room staff.

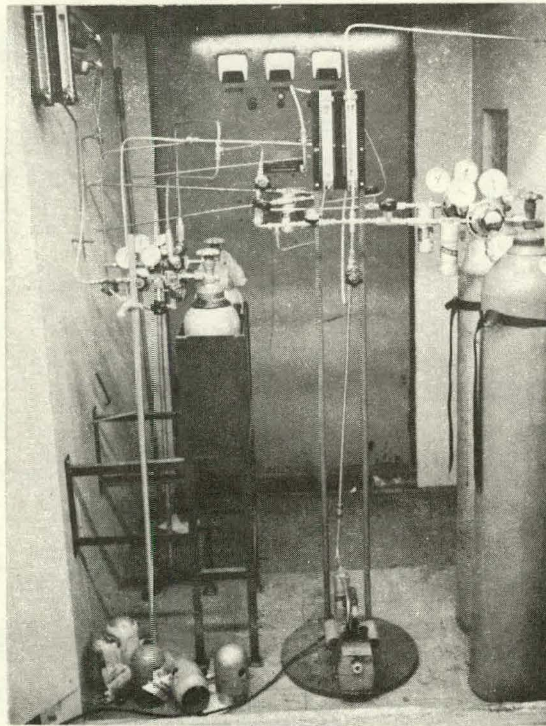

Figure 6. Walk-In Hood Containing the Gases and Gas Handling System.

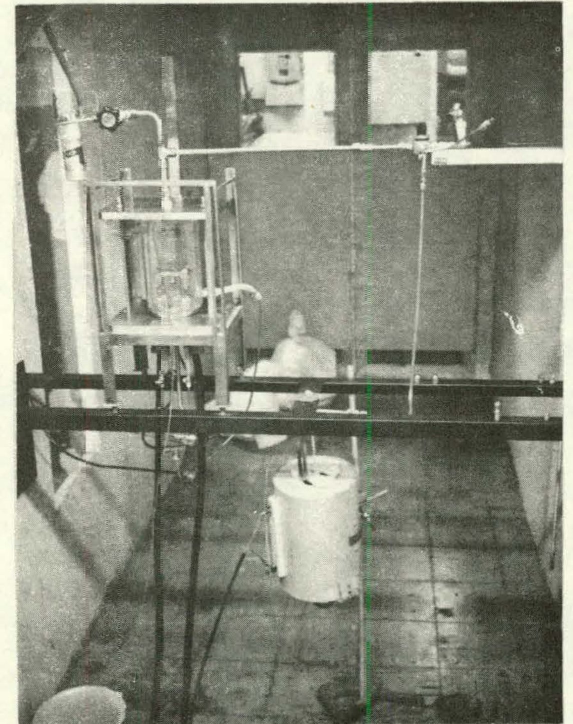

Figure 7. Walk-In Hood Containing the Deposition Reactor

1.4 CALIBRATION OF THE DEPOSITION SYSTEM

Calibration of the flowmeters used to measure the reactant and carrier gases proceeded smoothly. However, problems were encountered in relating the temperature of the substrate surface to that read by the controlling thermocouple. For convenience in design, the controlling thermocouple was placed directly beneath the Grafoil heater strip. The initial plan was to use very small surface thermocouples, temporarily placed in contact with the deposition surface, to calibrate this surface's temperature with that read by the controlling thermocouple. However, this did not work because the thermocouples were cooled far below the substrate surface temperature by the flow of argon. Therefore, all calibration is done at the time of deposition by measuring the deposition surface temperature with an optical pyrometer. This reading is not corrected for absorption by two thicknesses of quartz or the cooling water that must be sighted through, but it does give the consistency necessary for repeatability.

The use of the optical pyrometer is a problem when transparent substrates such as quartz and sapphire are used. The readings taken are highly influenced by the transmission of the visible light from the Grafoil heater strip. It is assumed that the temperature read by the optical pyrometer when viewing these substrates is near that of the heater strip and this temperature is probably considerably above the actual temperature of the upper substrate surface.

Even though the actual deposition surface temperature cannot presently be measured for transparent substrates, it is felt that the

readings are reproducible. However, one problem with this approach is that uniformity of the surface temperature cannot be determined as was done for silicon. This may be a problem since there are indications that the uniformity is reduced when hydrogen is used as the carrier gas, which is currently the case. Other methods are being investigated in an attempt to solve this problem.

2. FILM GROWTH

The film growth to date can be divided into three phases. The initial phase involved the use of only diborane (no arsine) to produce boron films. This phase was primarily used as a system check to ensure the safety of the design, to calibrate and check deposition parameters, to develop an effective substrate preparation technique, and to test the reproducibility of the equipment. Because the β-rhombohedral phase of boron thin films may also be of interest, it was initially hoped that experience could be gained which might prove worthwhile in later efforts. The second phase of the depositions used both diborane and arsine in attempts to deposit boron arsenide films with ultra high purity argon as the carrier gas. This approach provided a safety margin over the use of hydrogen and was expected to give information about the differences in deposition parameters and results for the two carrier gases. Deposition using hydrogen as the carrier gas was the third phase.

2.1 DIBORANE DEPOSITIONS

The depositions of boron from diborane comprise the first seven experimental runs. Even through the β-rhombohedral phase of boron is favored at temperatures of 1300°C and higher, the deposition temperatures used were below 1000°C in order to stay near the expected deposition temperatures of BAs. These experiments were mainly a system test.

The two substrate materials used were (111) oriented single crystal silicon and optical grade, fused quartz. The carrier gas in all cases was ultra high purity argon and all substrates were subjected to approximately a 900°C hydrogen in-situ etch immediately prior to deposition.

The first three depositions were on silicon substrates and the last four were on the quartz. The deposition conditions and the results of optical microscope examination are given in Table I.

None of the deposits on silicon resulted in a film type growth. The only deposit of appreciable thickness was that of deposition #1. This effort resulted in a columnar structure growth that either was not extremely adherent to the silicon or fractured the silicon surface. SEM photographs, as presented in Figures 8 and 9, show a few outstanding features in the deposit such as the hair-like columnar growth to the globular structures. X-ray results indicated this deposit to be rhombohedral boron. However, this could be due to only part of the deposit, since the non-uniformity of the structure indicates the phase could also be non-uniform over the surface.

Deposition #2 resulted in only a partial covering of the substrate. The deposit was more in the form of an uneven globular growth with some faceted crystalline structure. The product was very thin and detection by x-ray diffraction was ruled out. The final deposition on silicon (#3) was unsuccessful, resulting in a film with an oily appearance covering less than half the substrate.

Even though the results of the initial boron depositions on silicon were unacceptable, it is now felt that the probable cause of this was in the lack of an effective substrate preparation. All silicon substrates were ground and lapped with .05 μm Linde B powder followed by various solvent rinses which are outlined in Table II. No chemical etch or polish to clean or smooth the surface was attempted. The addition of

TABLE I

DIBORANE DEPOSITION PARAMETERS AND RESULTS

Deposition #	Diborane Flow Rate	Argon Flow Rate	Substrate Material	Deposit Time	Deposit Temp.	Optical Microscope and SEM Examinations
1	6.5mℓ/min.	3.7ℓ/min.	p-silicon	120 Min.	885-920°C	Very rough non-uniform coating. Chipped in one corner. Deposit cracked in places. Consists of vertical, hair like growths in some regions. Many different structures visible.
2	1.1mℓ/min.	3.7ℓ/min.	p-silicon	84 Min.	950°C	Coating rough with uneven globular growth but smoother than #1. Also much thinner. Only partial coating of the substrate.
3	1.1mℓ/min.	3.7ℓ/min.	p-silicon	62 Min.	940-970°C	Very thin. Oily appearance. Covers less than 1/2 the substrate. Probably not a boron film.
4	0.2mℓ/min.	17.5ℓ/min.	Quartz	100 Min.	$\sim$980°C	No visible deposit
5	7.9mℓ/min.	25ℓ/min.	Quartz	10 Min.	$\sim$900°C	Very thin. Semi-transparent. Metallic surface with roughness.
6	7.9mℓ/min.	25ℓ/min.	Quartz	13 Min.	$\sim$910°C	Shiny metallic film with cracks. Thicker than #5.
7	7.9mℓ/min.	25ℓ/min.	Quartz	27 Min.	$\sim$910°C	Thicker than #6. Rough in spots on a shiny uniform layer. Film is severly buckled.

a chemical polish and improved cleanliness of the operation may make boron film deposition on silicon feasible.

The remaining depositions were on fused quartz. The surfaces of these films were far superior to those deposited on silicon and the uniformity of the film thickness was also improved. Most deposits had a shiny metallic finish with few features. Some of these results may be due to the substrate material, but it should also be noted that some modifications in procedures and equipment were also made. The main cause of the improvement in thickness uniformity was a modification of the gas inlet system that allowed the reactant and carrier gases to enter the chamber in a 1" diameter tube instead of a 3/8" diameter tube. The surface quality may have been improved by the fact that the quartz was etched in a 1:2 HF in H_2O solution prior to solvent rinsing and insertion into the reaction chamber. Another improvement in surface quality was achieved by not mechanically polishing the deposition surface of the quartz substrates, since they were finely polished as purchased. The temperature values obtained by an optical pyrometer focused on the substrate are probably biased due to the transmission of visible radiation from the Grafoil heating strip through the quartz substrate. Therefore, the optical pyrometer readings shown in Table I were taken from the lavite mask of identical thickness directly adjacent to the substrate. The pyrometer readings obtained using silicon as the substrate indicate that this is a good approximation of the upper surface substrate temperature. However, due to differences in thermal conductivity of the silicon and quartz, the discrepancy is not known but is not felt to be large.

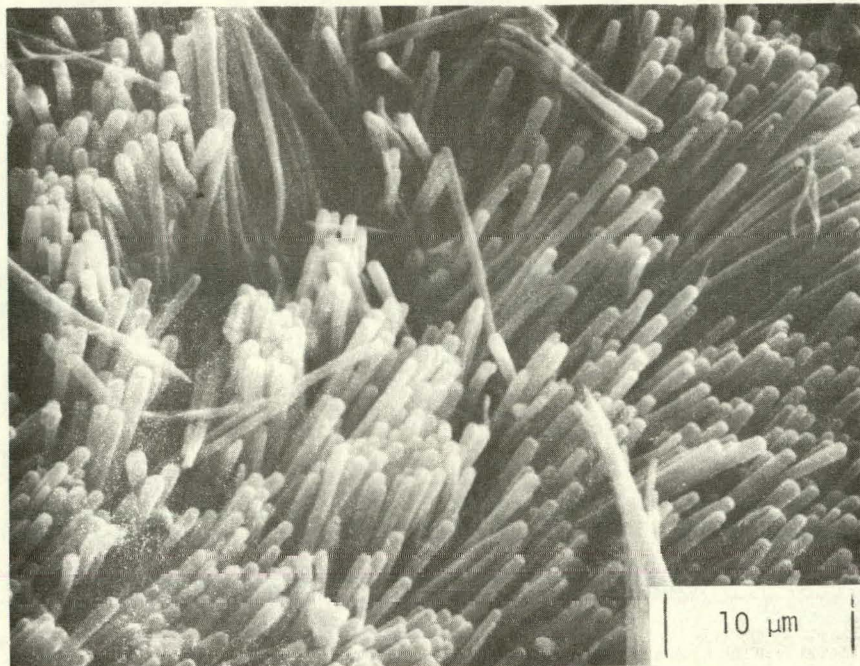

Figure 8. SEM photograph of Boron Deposition #1 (2500X).

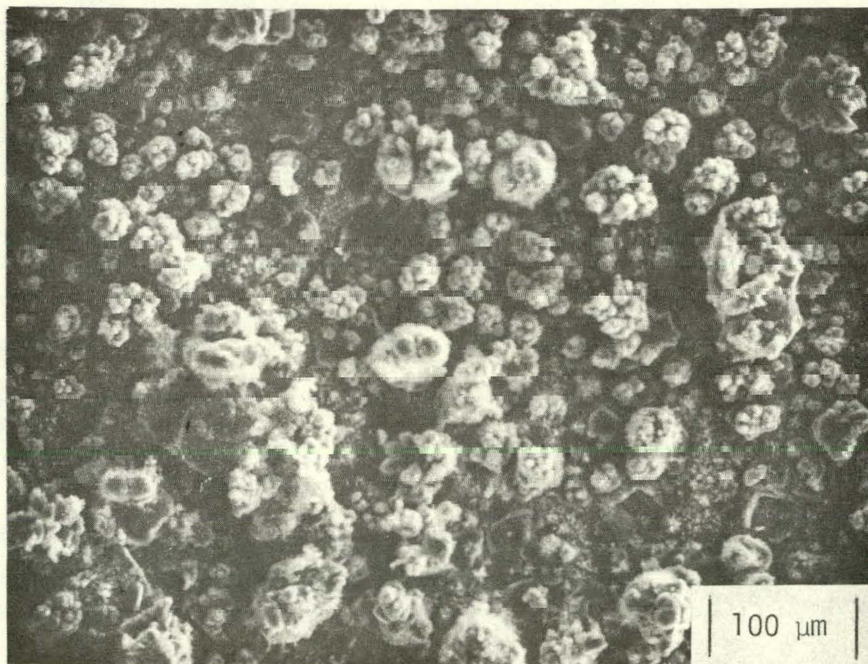

Figure 9. SEM Photograph of Boron Deposition #1 (200X).

TABLE II

SUBSTRATE PREPARATION TECHNIQUES FOR DIBORANE DEPOSITIONS

Deposition #	Substrate Material	Preparation
1	p-silicon	.05 μm Linde B polish; hexane rinse; alternating DI water - methanol rinses ending with DI water. 890°C H_2 etch for 30 minutes.
2	p-silicon	Same as #1
3	p-silicon	Same as #1 except final rinse in trichloroethylene (TCE)
4	Quartz	.05 μm Linde B polish; TCE rinse; DI water rinse; 3 minutes each in 1:2 HF: DI water; TCE rinse; DI water rinse; 30 minutes H_2 etch at 850°C
5	Quartz	Same as #4
6	Quartz	Same as #'s 4 and 5 except deposition surface was not polished at Eagle-Picher, manufacturer's polish was used.
7	Quartz	Same as #6

The use of quartz as an effective substrate for boron deposition has been ruled out, however, since the thicker deposits (#'s 6 & 7) severely buckled upon cooling indicating a large thermal coefficient of expansion mismatch.

At this point it must be re-emphasized that this was only a precursory examination of boron deposition and no concerted efforts to deposit high quality films, find an effective substrate, or evaluate the films electrically and optically were made.

2.2 DIBORANE - ARSINE DEPOSITIONS

Eleven depositions have been carried out with both diborane and arsine in attempts to produce crystalline films of BAs. Special emphasis was placed on substrate materials that were compatible with both the electrical and optical measurements. This condition would allow nearly complete characterization of the films without removal from the substrate; a considerable task. Two substrate materials have been used which satisfy both characteristics, fused quartz and (0001) oriented single crystal sapphire (Al_2O_3). A small substrate of hot pressed SiC was also used for one deposition (#14). A thorough evaluation of this substrate material was not possible because of the lack of enough substrates. Although hot pressed SiC would be useable for the electrical characterizations, it will not allow optical absorption measurements of the films. Epitaxial growth was not expected on any of the substrates due to their polycrystalline (SiC) or amorphous (quartz) nature or because of lattice mismatch (Al_2O_3).

Quartz was the initial substrate material (#8) investigated. It is highly insulating, enabling film electrical characterization to be made on the substrate, and is transparent from the visible down to approximately 4 μm (∿0.3eV). The substrate was prepared as for boron depositions on this material (see Table III). The deposition was carried out in argon and the conditions of deposition whereas shown in Table IV. A very shiny thin film was produced similar to that for boron. The film cracked severely, even though the cool-down of the film and substrate was done carefully and slowly. This has been interpreted as a mismatch in the thermal coefficients of expansion of the two materials and no further attempts were made to deposit on fused quartz.

All other depositions, with the exception of #14, have been carried out on (0001) oriented single crystal sapphire. This material is also highly insulating and transmits down to 6 μm (∿0.2 eV). Apparently there is no problem with mismatch of the thermal coefficients of expansion of the two materials since two films (#'s 15 and 16) cooled from the deposition temperature (near 900°C) to near ambient temperature in less than one minute due to a temperature controller malfunction and no cracks or peeling could be detected in the resultant films. The procedures for preparing the sapphire substrate surfaces are summarized in Table III. The deposit surface was not mechanically ground since the as received surface was sufficiently smooth. The chemical polish with sulfuric and phosphoric acid at 200°C and the subsequent solvent cleaning in a heated ultrasonic cleaner apparently gave good deposition surfaces with highly adherent films with the exception of #'s 12 and 13. In these two depositions there was apparently a problem with chemical contamination

TABLE III

SUBSTRATE PREPARATION TECHNIQUES FOR DIBORANE-ARSINE DEPOSITIONS

Deposition #	Substrate Material	Preparation
8	Fused Quartz	TCE rinse; DI water rinse; 3 minute etch in 1:2 HF: water; rinses in DI water, TCE, DI water; no mechanical polish, 30 minute H_2 etch at 750°C
9	Sapphire (0001) .040"	Alternating rinses in TCE and DI water ending with DI water; 10 minutes H_2 etch at 860°C, no mechanical polish.
10	Sapphire (0001) .040"	Solvent rinse; DI water rinse; 15 minute chemical polish in 1:1 sulfuric and phosphoric acid at 200°C; 2 DI water rinses; H_2 etch at 920°C for 30 minutes.
11	Sapphire (0001) .040"	Same as #10 except final rinse in TCE and loaded into the reactor while still wet with TCE.
12	Sapphire (0001) .040"	Same as #11
13	Sapphire (0001) .040"	Same as #11
15	Sapphire (0001) .025"	Ground back side. Solvent rinse; DI water rinse; 15 minute chemical polish in 1:1 sulfuric and phosphoric acid at 200°C; DI water rinse; 2 methanol rinses; loaded into the reactor while still wet with methanol. 30 minute H_2 etch at 1100°C.
16	Sapphire (0001) .022"	Same as #15 except H_2 etch at 1000-1050°C for 25 minutes.
17	Sapphire (0001) .022"	Same as #15 except H_2 etch of 975-1050°C for 30 minutes.
18	Sapphire (0001) .022"	Same as #15 except H_2 etch of 925-995°C for 15 minutes.

TABLE IV

DIBORANE-ARSINE DEPOSITION PARAMETERS AND RESULTS USING ARGON AS THE CARRIER GAS

Deposition #	Diborane Flow Rate	Arsine Flow Rate	Argon Flow Rate	Substrate Material	Deposit Time	Deposit Temp.	Optical Microscope Examinations
8	3.6mℓ/min.	16.0mℓ/min.	25ℓ/min.	Fused Quartz .025"	20 Min.	∿900°C	X-ray: Amorphous Very shiny thin film crossed with a multitude of cracks; some deposit roughness noted.
9	3.6mℓ/min.	16.0mℓ/min.	30ℓ/min.	Sapphire (0001) .040"	60 Min.	∿990°C	X-ray: $B_{13}As_2$ Thin film; appears no thicker than #8; shows evidence of insufficient substrate preparation; brownish in color; semi-transparent
10	3.6mℓ/min.	16.0mℓ/min.	25ℓ/min.	Sapphire (0001) .040"	60 Min.	∿860°C	X-ray: Amorphous Shiny, metallic film, transmits red light.
11	3.6mℓ/min.	16.0mℓ/min.	25ℓ/min.	Sapphire (0001) .040"	60 Min.	∿920°C	X-ray: Amorphous Shiny metallic film, thicker than that of #10; small globules visible on the surface with some very tall; transmits red light. 10 μm thick.
12	3.6mℓ/min.	16.0mℓ/min.	25ℓ/min.	Sapphire (0001) .040"	120 Min.	∿940°C	X-ray: Amorphous Non-adherent, shiny, grey film; apparently insufficient substrate preparation; thickest film yet.
13	3.6mℓ/min.	9.2mℓ/min.	25ℓ/min.	Sapphire (0001) .040"	60 Min.	∿965°C	X-ray: $B_{13}As_2$; very shiny film; transmits red; adhesion very poor because of insufficient substrate preparation.

since the films were not totally adherent. Film #12 was nearly totally non-adherent and continued to flake off while #13 had only three small non-adherent regions. The inadequacy of the substrate preparation was detected optically on both films before loading them into the reactor. A further improvement in cleanliness resulted from loading the substrate into the reactor while still wet with solvent (either trichloroethylene or methanol) from the last ultrasonic rinse. Film adhesion seems to be as good with this technique as when the substrate was allowed to dry before loading and the number of foreign particles present on the substrate prior to deposition has decreased drastically. All substrates were also subjected to a hydrogen etch at 800-1100°C before deposition as outlined in Table III. Depositions #'s 9-13 were carried out at temperatures ranging from 860°C to 990°C with argon as the carrier gas. These temperatures are optical pyrometer readings taken on the transparent substrate and are probably higher than the temperature of the deposition surface. The deposition parameters are given in Table IV. In all cases the arsine flow was higher than the diborane flow by at least a factor of two to provide some excess of arsenic. At this point the only influence of deposition parameters on the crystallinity of the films is that the higher temperatures (above 965°) produced crystalline boron subarsenide while the lower temperatures (940° and below) produced amorphous material.

The thinnest films produced (9, 17, and 18) are brownish in color and semitransparent. The thicker films have a shiny, metallic finish and transmit in the red. The surfaces of the films exhibit no crystalline features under high magnification using the scanning electron microscope.

The SEM photographs shown in Figures 10-13 are typical of all the films produced to date. A scraped edge of each film is shown in Figure 10 for film #11 and Figure 12 for film #13. With the scale shown, the thickness of film #11 was estimated to be 10 μm, and that of #13 to be 8 μm.

Films #'s 15-18 were grown using hydrogen as the carrier gas. The deposition conditions and results are listed in Table V. Films #'s 15 and 16 have a shiny, metallic finish like most of the films produced in argon and they transmit in the red. They initially grew by forming visible islands rather than a uniform layer over the whole surface as displayed by the films grown in argon. Films #17 and 18 were grown at low temperatures (770° - 790^oC) and are brownish in color, and very thin. Film #17 shows definite non-uniformity in the film thickness with the heavier deposit near the center.

Film #15 shows 2 small red crystals embedded in the film when viewed by an optical microscope. This is the only film to exhibit this. There is a good possibility that these are boron crystals (probably the low temperature form, "red" boron). Film #15 also shows crystalline boron by x-ray diffraction although the phase cannot be identified. Film #16 possibly shows crystalline boron by x-ray diffraction but also exhibits a broad amorphous peak. Films #17 and 18 have not been completely analyzed by x-ray diffraction at this time. All other films give similar amorphous x-ray diffraction patterns.

Because amorphous films do not exhibit definitive characteristic peaks, the identity of the chemical composition of these films is not readily discernable from the x-ray diffraction results. However, there are indications that the films do contain arsenic as a major component

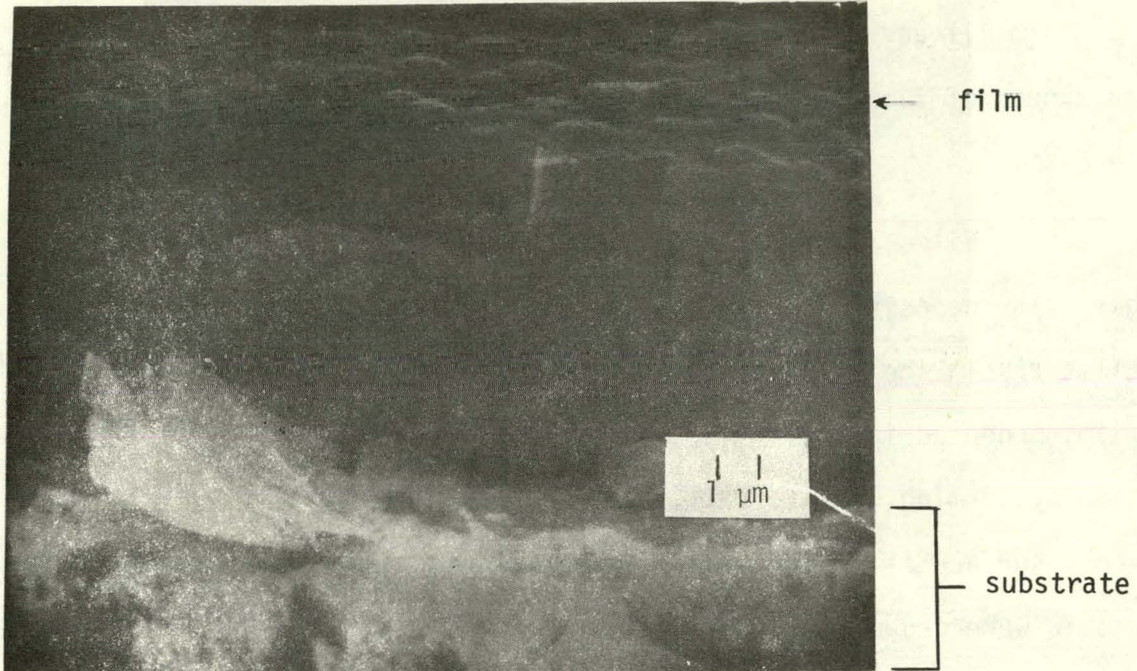

Figure 10. SEM Photograph of Edge of Film #11 (5000X).

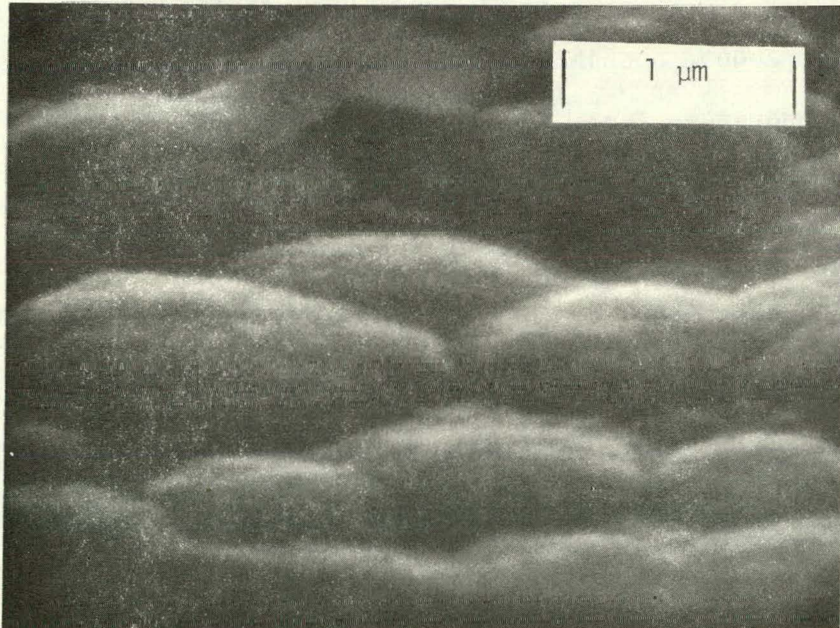

Figure 11. SEM Photograph of Surface of Film #11 (30,000X).

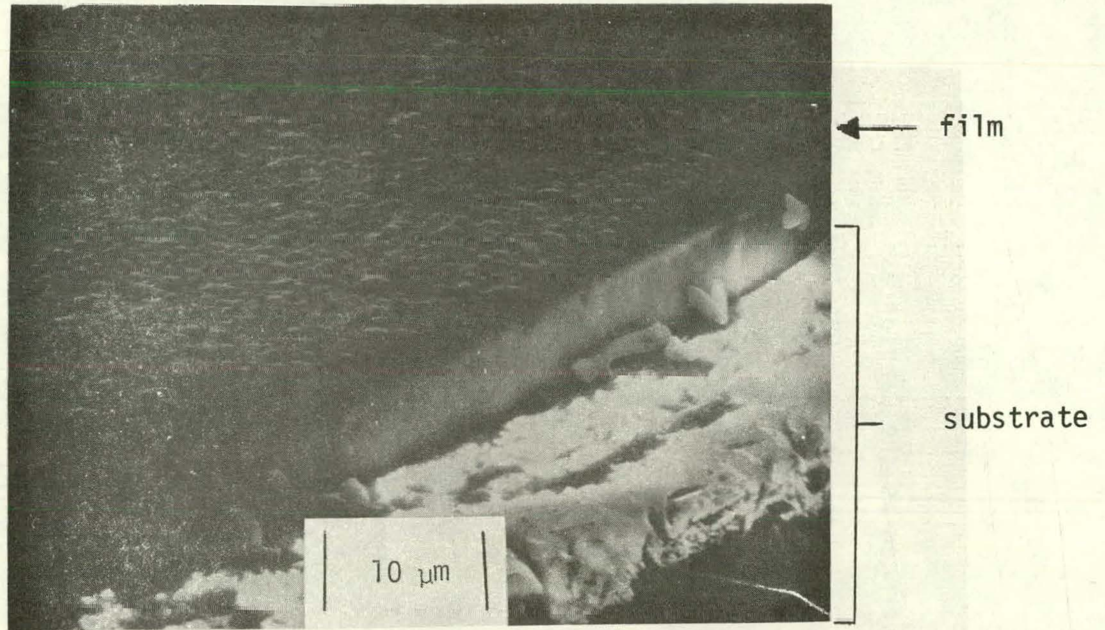

Figure 12. SEM Photograph of Edge of Film #13 (1500X).

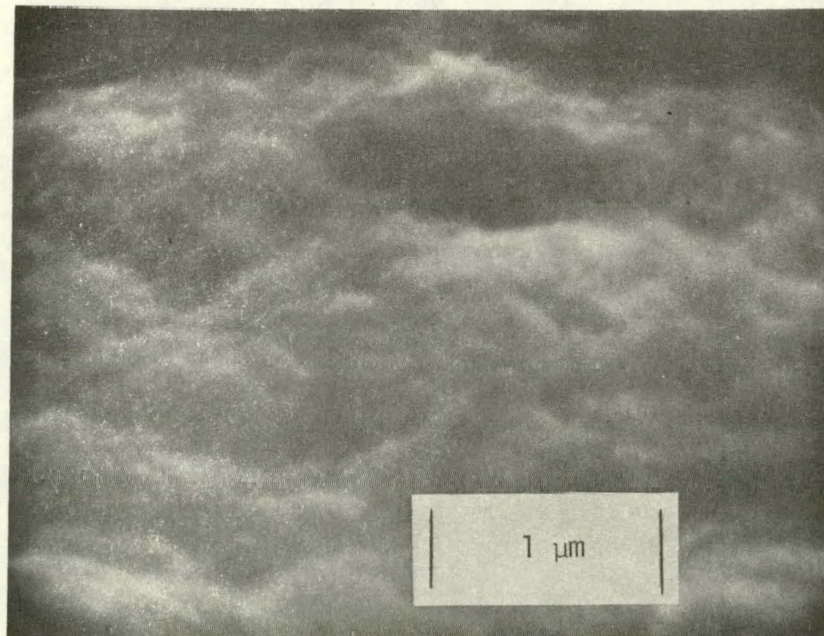

Figure 13. SEM Photograph of Surface of Film #13 (30,000X).

TABLE V

Diborane-Arsine Deposition Parameters and Results Using Hydrogen as the Carrier Gas

Deposition #	Diborane Flow Rate	Arsine Flow Rate	Hydrogen Flow Rate	Substrate Material	Deposit Time	Deposit Temperature	Results
15	3.6 mℓ/min	18.3 mℓ/min	35 ℓ/min	Sapphire (0001) .025"	25 min	∿ 855-870°C	X-ray: mainly boron shiny film; transmits red; 2 small red crystals embedded in film
16	3.0 mℓ/min	15.0 mℓ/min	15 ℓ/min	Sapphire (0001) .022"	22 min	∿ 875-905°C	X-ray: possible boron, mainly amorphous; shiny film; transmits red
17	1.44 mℓ/min	15.0 mℓ/min	10 ℓ/min	Sapphire (0001) .022"	40 min	∿ 775-790°C	X-ray: not completed very thin; non-uniform thickness; brownish in color
18	1.44 mℓ/min (45 min) 3.0 mℓ/min (40 min)	15.0 mℓ/min (45 min) 30 mℓ/min (40 min)	21 ℓ/min	Sapphire (0001) .022"	45 min & 40 min	∿ 770-785°C	X-ray: not completed thicker than #17 but still thinner than shiny metallic films; uniformity improved

since the films are thin enough that the x-ray beam may not be totally absorbed before reaching the sapphire substrate.

Because arsenic has a much higher mass absorption coefficient than boron for CuKα radiation, (76.5 $\frac{cm^2}{gm}$ as compared to 3.06 $\frac{cm^2}{gm}$) major sapphire x-ray diffraction lines should be significantly more apparent with thin films of low arsenic concentration than those of higher arsenic concentrations. No sapphire peaks were detected in the 10 μm thick film, #11, that was amorphous. This could be an indication that the films had a high arsenic concentration, possibly enough to be amorphous BAs. However, since the substrates are single crystal, the absence of sapphire lines may also be due to a chance misalignment of the sapphire diffracting planes with the x-ray beam. An effort will be made in the next quarter to investigate this by modifying the x-ray diffraction technique to allow a relative measurement of the intensity of sapphire lines on both the front and back side of the substrate.

Although no crystalline films of BAs have been produced at this time, the parameter variations have not been completely explored and work with the variation in temperatures is continuing.

3. OPTICAL AND ELECTRICAL MEASUREMENTS

3.1 OPTICAL MEASUREMENTS

Spectrophotometer tests have been performed on samples #9, #11, #13, and #16, with a thorough analysis nearly complete only on samples #11 and #13. We are presently hindered by the fact that the equipment we are using lacks a critical range of wavelengths ($0.75\ \mu m < \lambda < 2.5\ \mu m$) which is necessary for definite conclusions regarding the magnitude and directness of the bandgap(s) and possible impurity effects. Arrangements are being made at both MRL and UMR to obtain absorption data in this key wavelength range. Calculations have been completed on samples #11 and #13 to obtain values of the optical absorption coefficient α, $(\alpha\ell)^2$ and $(\alpha\ell)^{0.5}$, where ℓ is the thickness of the sample film. The wavelength sensitivity of the reference beam attenuators have been included where appropriate. The data was obtained in the infrared range from 2.5 μm to 6 μm, in the visible range from 750 nm to 350 nm, and in the ultraviolet range from 360 nm to 200 nm. Due to large variations in the characteristics of the reference beam attenuators in the ultraviolet range, possibly introducing errors, we are suspicious of this data and have not included it. Infrared data for wavelengths greater than 6 μm are not obtainable due to absorption in the sapphire substrate. Figures 14, 15, 16 and 17 are the raw data sets obtained from the spectrophotometers. The infrared data in Figures 14 and 15 show a small gradual change in transmittance. The main results of interest are the "quasi-sinusoidal" fluctuation in transmittance due to constructive and destructive interference from internal reflections in the films. The wavelength values of these extrema

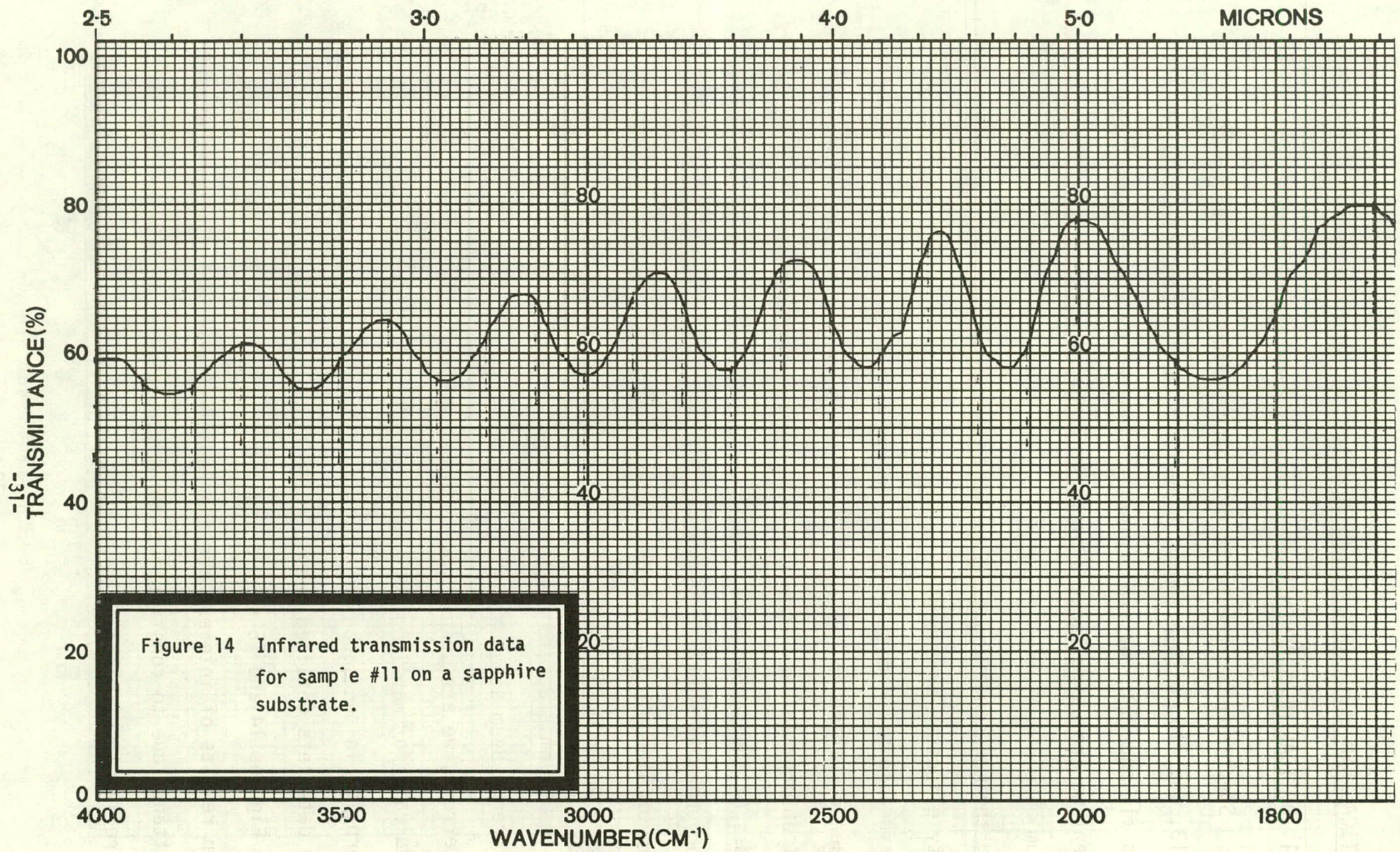

Figure 14 Infrared transmission data for sample #11 on a sapphire substrate.

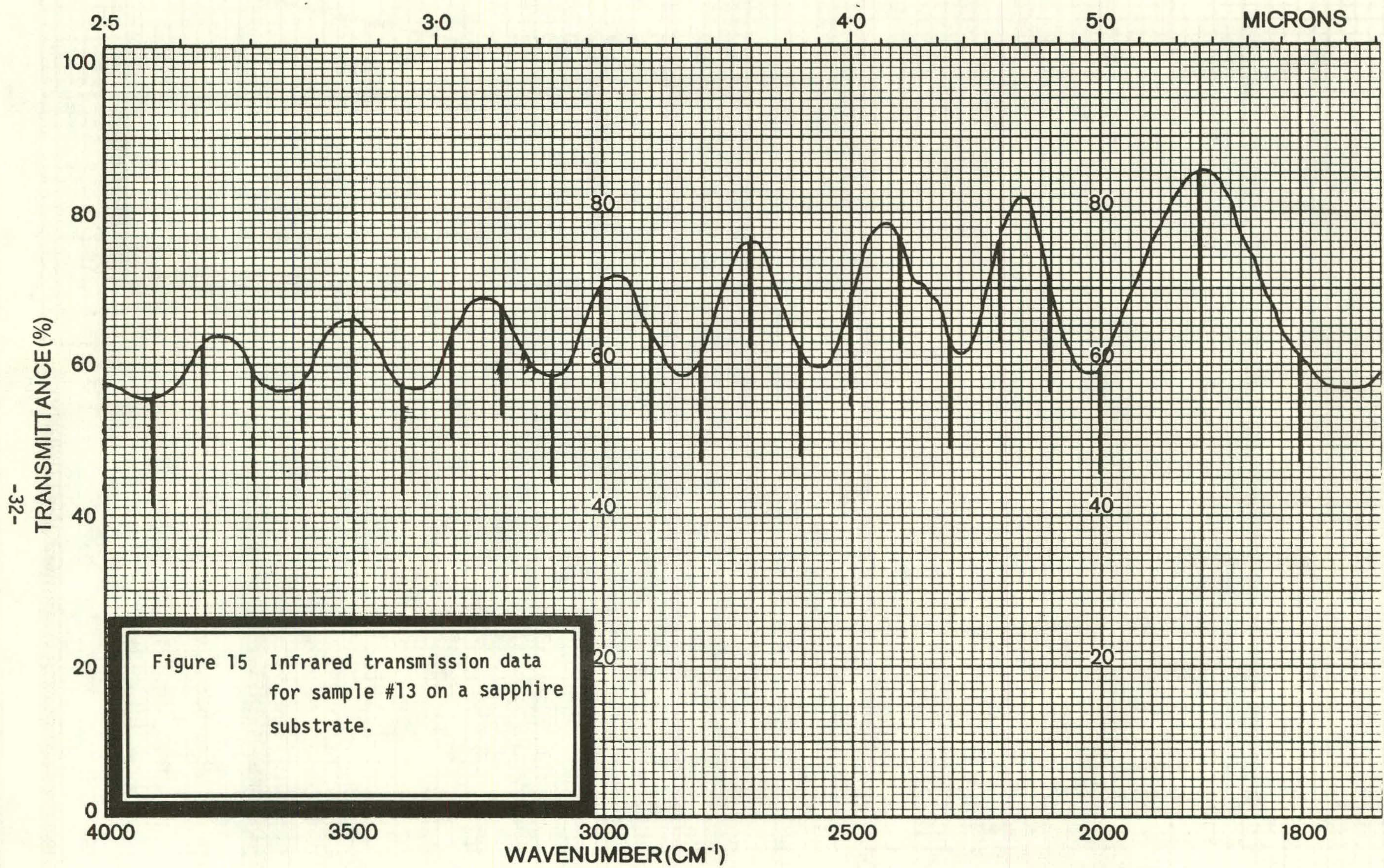

Figure 15 Infrared transmission data for sample #13 on a sapphire substrate.

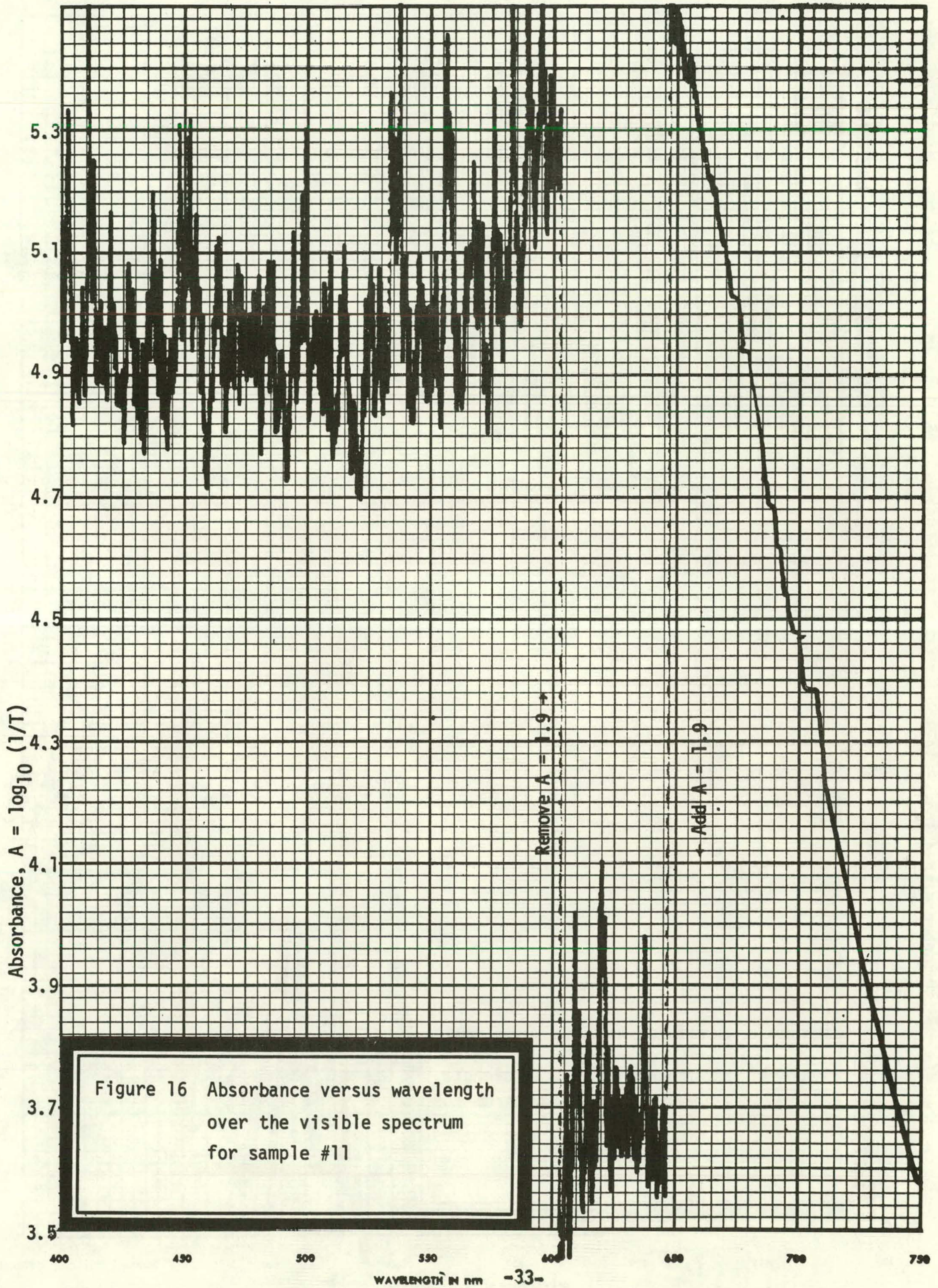

Figure 16 Absorbance versus wavelength over the visible spectrum for sample #11

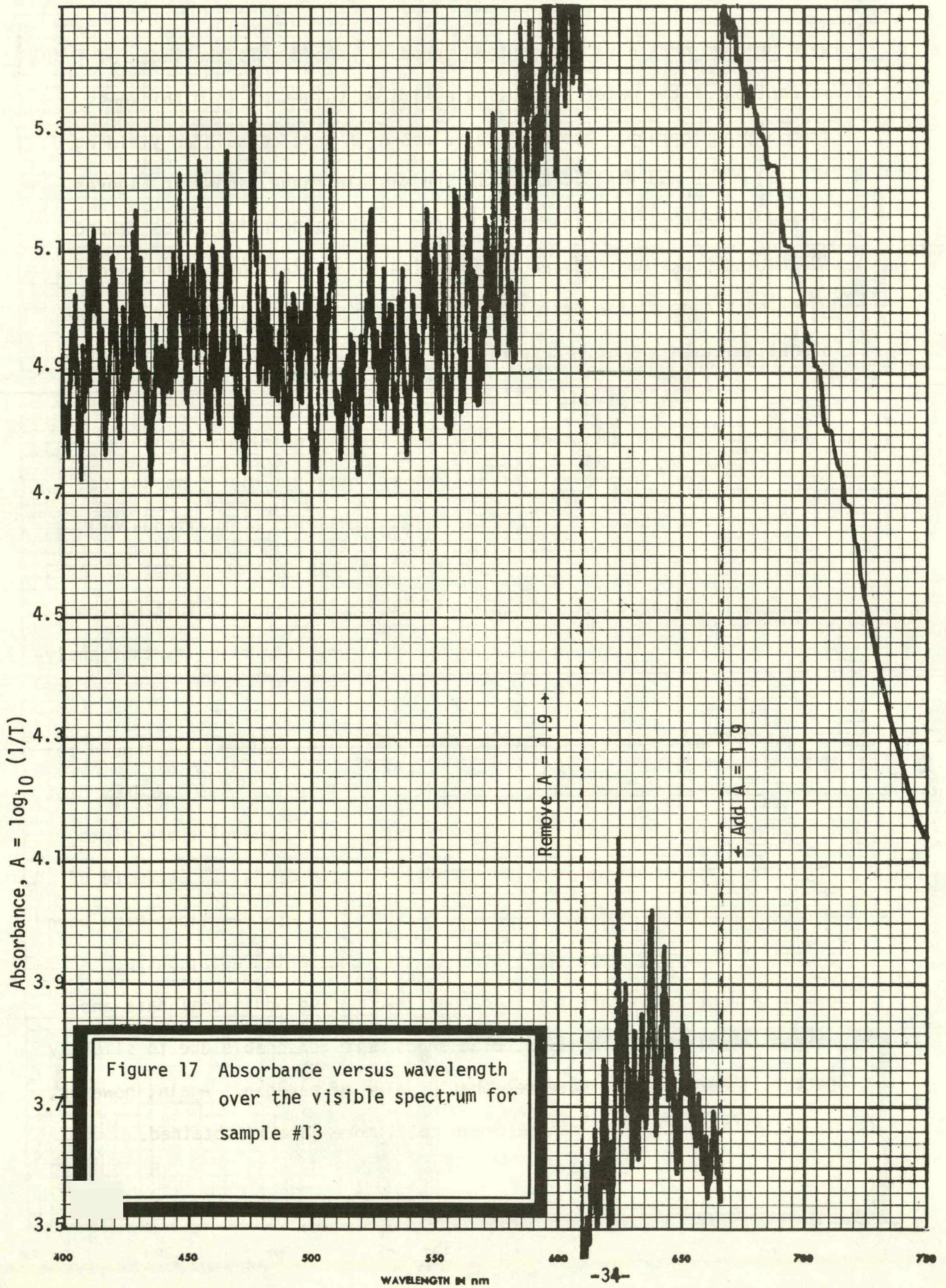

Figure 17 Absorbance versus wavelength over the visible spectrum for sample #13

were used to obtain values of the $\eta \ell$ product, where η is the index of refraction of the material. Using estimated values of film thickness from SEM photographs, approximate values of η were calculated yielding η (#11) $\approx$ 1.8 and η(#13) $\approx$ 2.3. In the visible range, shown in Figures 16 and 17, one notices the steep slopes of the absorption edges around 700 nm and peaks near the edge. The significant fall off on the short wavelength side of the peak is somewhat suprising and lacks a clear explanation at this time. Referring to Figure 18, it is evident that the magnitude of α is in the upper 10^3 cm^{-1} to lower 10^4 cm^{-1} range, which is a reasonable value. Another interesting feature on Figure 18 is the short wavelength "climb" at the edge of the graph. This is masked on the raw data by the strong rise in filter (reference beam attenuator) absorption. The value of α rises up to the middle 10^4 cm^{-1} range and indications are that it will continue to rise even farther. This may be due to a second bandgap or an effect of the very thin film; further analysis is needed.

Theory indicates that an α^2 versus photon energy plot should be linear for direct gap material and that an $\alpha^{0.5}$ versus photon energy plot should be linear for indirect gap materials. Also, one of these plots should cross the energy axis at the material bandgap, so an estimate of the bandgap can be made. On Figures 19 and 20, these functions have been plotted. Both appear fairly linear at the fundamental edge, but a definite conclusion cannot be made until we obtain additional data and extend the "lines." The $(\alpha \ell)^2$ plot seems more reasonable due to slightly better linearity and a more reasonable value of bandgap. Again, however, no definite conclusions can be drawn until more data is obtained.

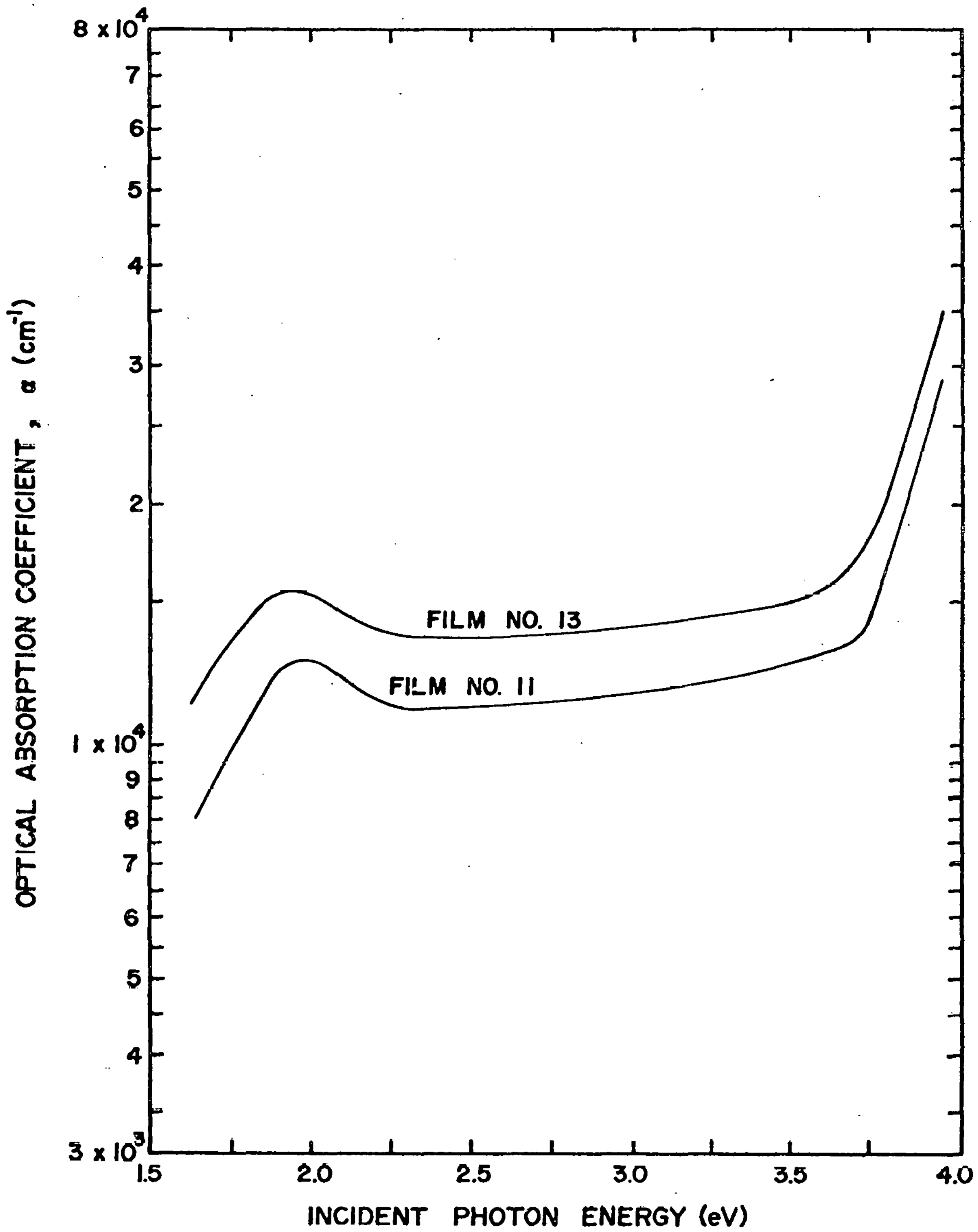

Figure 18. Absorption Coefficient vs. Incident Photon Energy for Films #11 and #13.

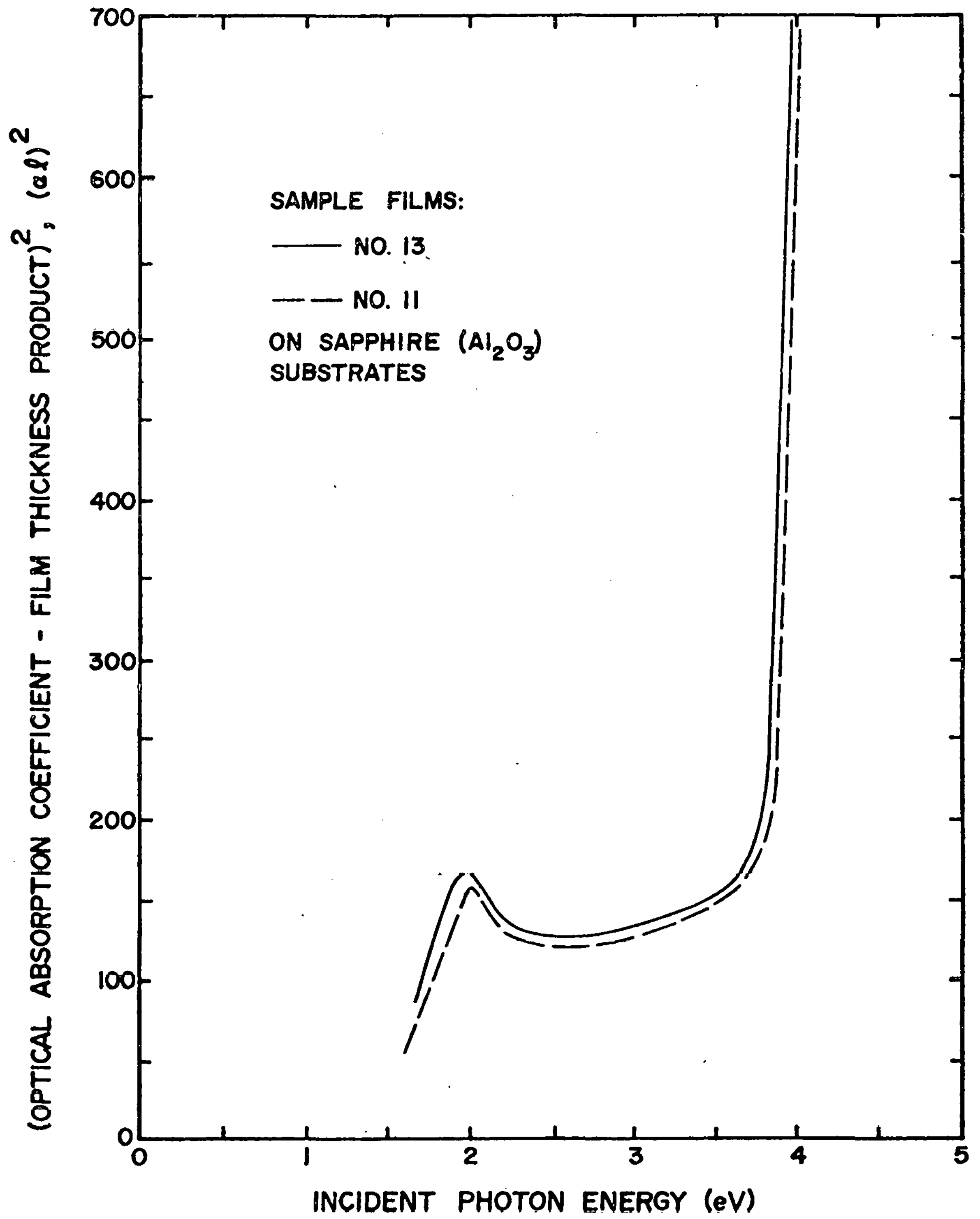

Figure 19. $(\alpha\ell)^2$ vs. Incident Photon Energy for Films #11 and #13.

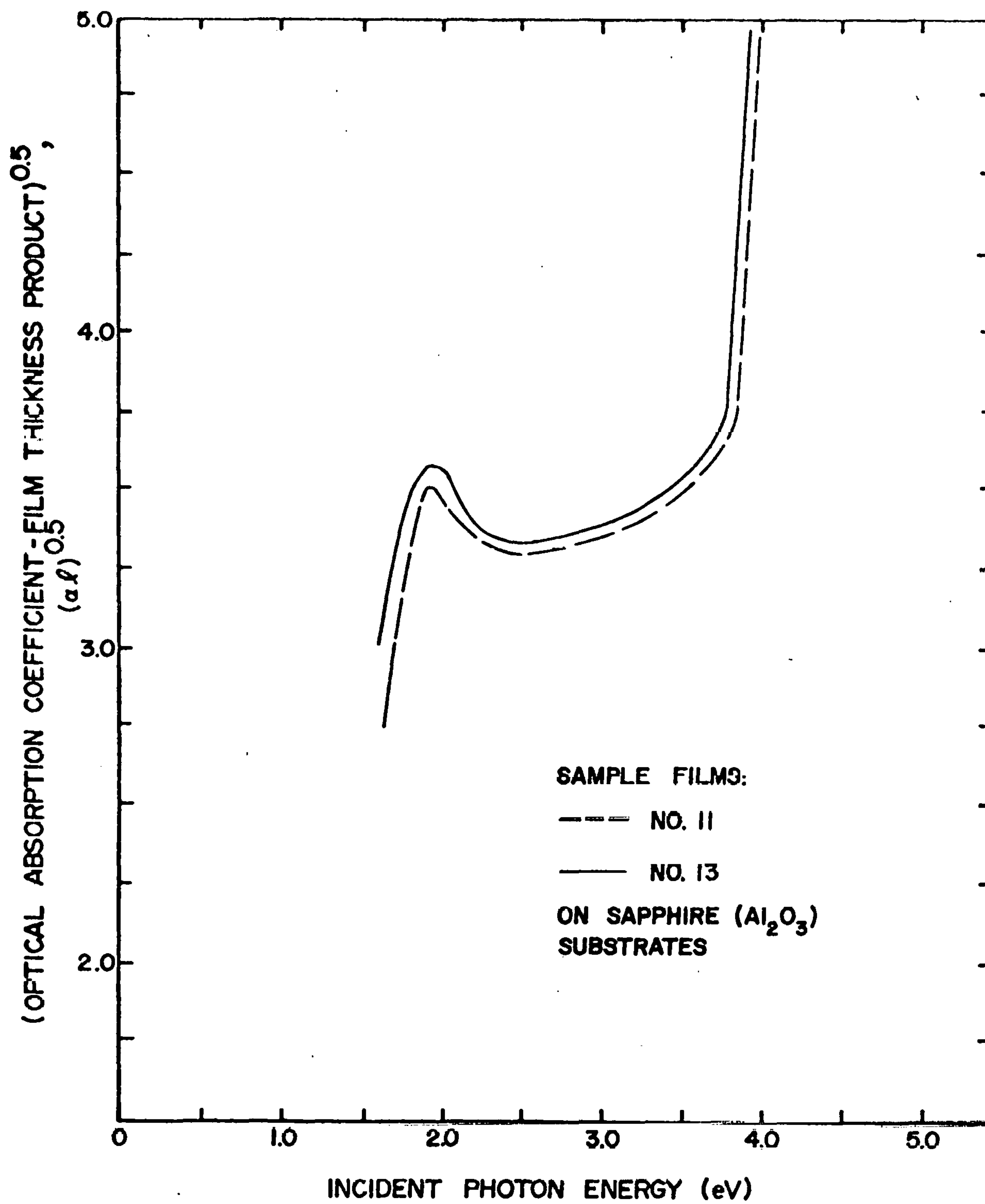

Figure 20. $(\alpha\ell)^{0.5}$ vs. Incident Photon Energy for Films #11 and #13.

3.2 ELECTRICAL CONDUCTIVITY MEASUREMENTS

In order to determine the room temperature conductivity, the four point probe method was used. The probe consists of four individually spring loaded pressure contacts arranged in a square array. When using a square array of contacts, current is passed through two probes along one side while the two remaining probes are used to measure the voltage which results from this current. For this type of arrangement, it can be shown that the conductivity is expressed as

$$\sigma = \frac{\ell n\sqrt{2}}{\pi t}(I/V) \qquad (\Omega cm)^{-1},$$

where σ = conductivity $(\Omega cm)^{-1}$
I = current through sample (A)
V = voltage due to current (V)
t = thickness of film (cm).

Samples #11 and #13 were investigated. The conductivity measurements were made with a magnitude of current low enough to prevent Joule heating of the film. Voltage measurements were made at several magnitudes of current. Current direction was then reversed and voltage readings were again recorded. The I-V data was taken at several locations on the film and averaged. The locations were chosen to eliminate effects from the edge of the film. Results obtained appear in Table VI.

Strip contacts were then applied along the width of sample #11. These contacts were made by the vacuum deposition of aluminum into strips. The sample was subsequently annealed at 450°C in argon for 12 minutes to achieve a good mechanical bond between the aluminum strip and the film. The aluminum was then overlayed with a highly conductive silver

SAMPLE NO.	FOUR POINT PROBE σ $(\Omega \text{ cm})^{-1}$	TWO POINT PROBE σ $(\Omega \text{ cm})^{-1}$
11	1.66×10^{-4}	1.55×10^{-4}
13	1.43×10^{-4}	

Table VI. Room Temperature Conductivity for Films #11 and #13.

paste, and when the paste was cured, good ohmic contacts had been formed.

The conductivity of sample #11 was measure using the strip contacts. This was done as a check on the four-point probe results obtained previously. Current was passed through the leads and the voltage measured across these same contacts. The conductivity was calculated using

$$\sigma = \left(\frac{I}{V}\right) \left(\frac{\ell}{s}\right) \qquad (\Omega\text{cm})^{-1},$$

where ℓ= length between the contacts (cm)

s = cross sectional area of film (cm^2).

The averaged results of the two-point probe method appear in Table VI. When comparing the results of the four-point probe and the two-point probe methods, remember that one method uses probe spacings on the order of millimeters while the other has a probe spacing on the order of centimeters. The results of these measurements support the visual observation that the film is uniform with an amorphous appearance (see Figure 11).

Sample #11 was used to make conductivity versus temperature measurements in an effort to determine the thermal energy gap. These measurements were made by increasing the temperature in increments. At each point, the sample was allowed to come to thermal equilibrium, and measurements were repeated with the current and voltage reversed to rule out instrument error.

Figures 21 and 22 are semilog plots of the conductivity versus 1/T for a range of temperatures from 77 K up to 890 K. It was hoped that this plot would provide some information relative to the energy gap and impurity content of the material.

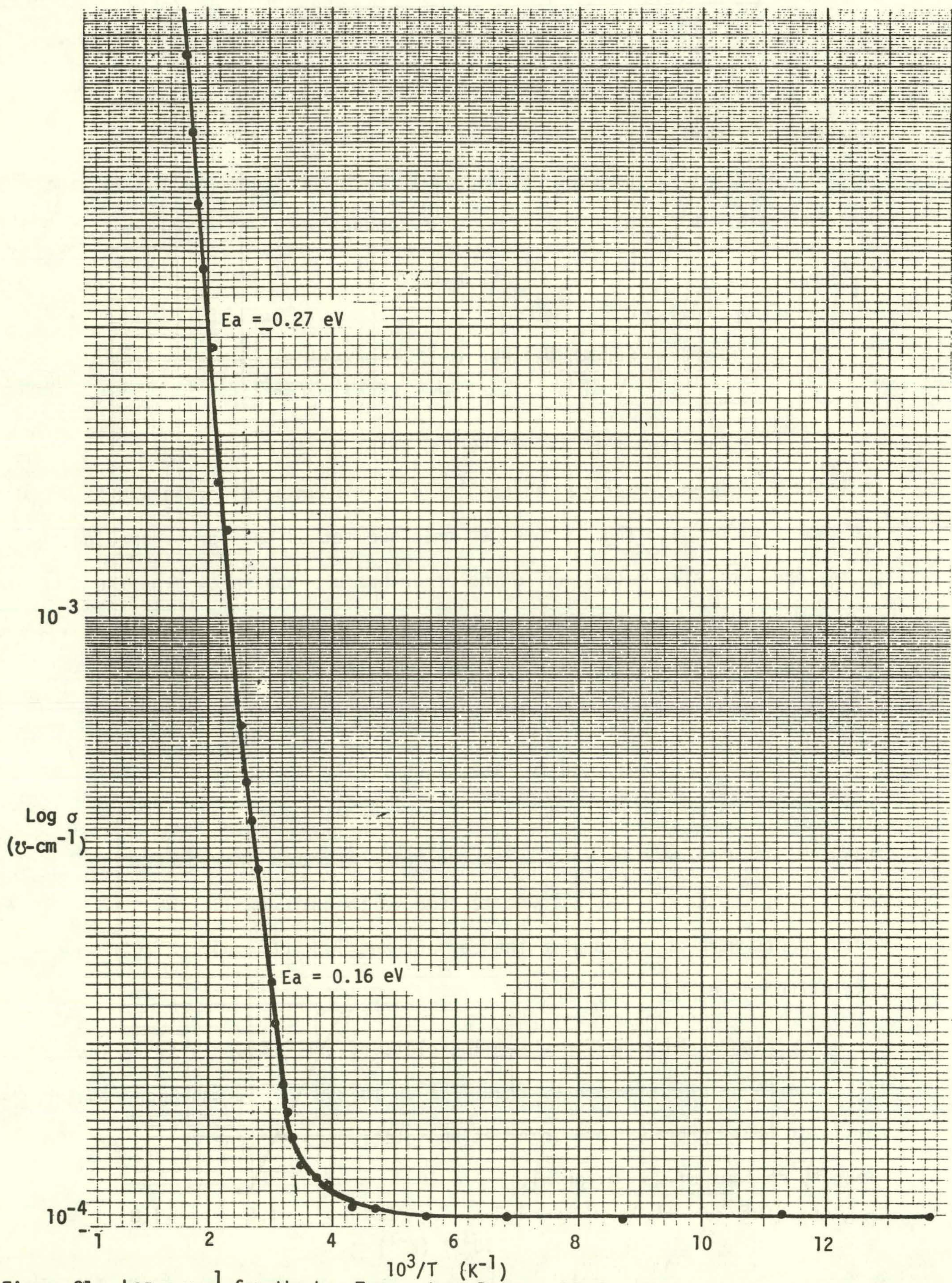

Figure 21. Log σ vs $\frac{1}{T}$ for the Low Temperature Range. Sample #11

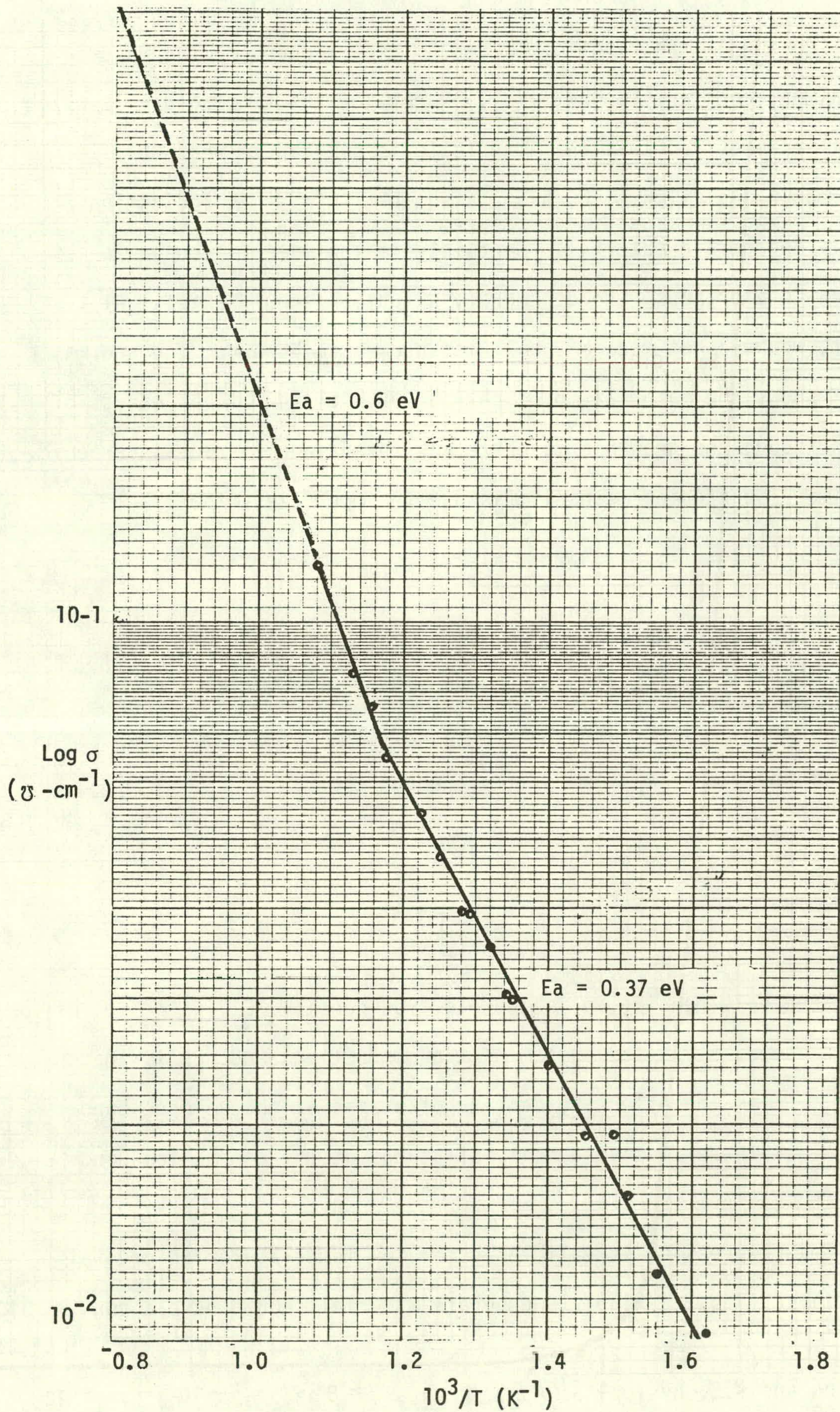

Figure 22. Log σ vs $\frac{1}{T}$ for the High Temperature Range. Sample #11.

Looking at the range of temperatures below 250 K, the material displays almost constant conductivity, except for the temperature at which the transition occurs. This characteristic is similar to what Chu (1) has observed in BAs films. Chu has stated that this is an indication of a highly degenerate material. Certainly if the material under investigation is amorphous, the degeneracy situation should exist. At this point, we have not made any Hall measurements; however, the thermal probe test shows the material to be p-type, probably due to an excess of boron even though the growth atmosphere was intentionally rich in arsenic. If the primary scattering mechanism is due to impurities, then:

$$\mu = \frac{T^{3/2}}{m^{*\frac{1}{2}} N_I},$$

where μ is the carrier mobility, T is temperature in Kelvin, m^* the effective mass, and N_I is the impurity density.

If the material is completely degenerate,

$$p = N_V \left[\frac{4}{3} \sqrt{\pi} \; (E_V - E_F)/kT \right]^{3/2}$$

$$n = N_C \left[\frac{4}{3} \sqrt{\pi} \; (E_F - E_C)/kT \right]^{3/2}$$

where p is the hole density, n is the electron density, E_V is the top of the valence bond, E_C is the bottom of the conduction band, E_F is the Fermi level, N_V is the effective density of states at the valence band edge, and N_C is the effective density of states at the conduction band edge.

This expression is valid only for low temperatures in crystalline materials. Thus, a highly degenerate material should have a con-

1. T.L. Chu and A.E. Hyslop, J. Appl. Phys., Vol. 43, No. 2, p. 276, Feb. 1972.

ductivity which has little dependence on temperature at low temperature. We are assuming that this is the situation for Sample #11. Indications are that the Fermi level may lie around 0.1 eV below the valence band edge (for p type) for T = 200 K. Figure 8 shows that for T>200 K the material starts to become less degenerate and at about 300 K the Fermi level will line up with the "band edge".

As the temperature is increased, the conductivity starts to increase exponentially due to an increase in carrier density. The exponential increases shown in Figures 8 and 9 indicate four activation energy levels between room temperature and 920 K. These levels have not been thoroughly explored and, due to the limited number of samples tested (one), we will not assume these to be "characteristic" energy levels. The log σ versus $\frac{1}{T}$ plot shows the possibility of trap levels at approximately 0.16, 0.27, 0.37, and 0.6 electron volts. This information at least supports the conclusion that the material is amorphous. The resistivity of the material decreases from about 10^4 ohm-cm to 10 ohm-cm over the range of these measurements. In the absence of any mobility measurements, we can not attribute this high resistivity to low mobility. However, the sample did not demonstrate photoconductivity when exposed to an intense tungsten source.

Further, the conduction mechanism has not been thoroughly analyzed although the observation of the activation levels would indicate that within the range of voltage and current used the material is ohmic. The V-I measurements reported here are limited primarily due to the absence of samples. This reflects the fact that the initial effort has been associated mainly with the growth of films. The essential observation we make at this point is that sample #11 does not display the properties we expect to ultimately achieve.

3.3 LIFETIME MEASUREMENT AND LIGHT SCANNING SYSTEMS

Work is presently being done with LED's and solid state lasers to obtain sufficiently intense and short light pulses to use the photoconductive decay method in obtaining estimates of minority carrier lifetimes for BAs. The lifetimes are anticipated to be in the lower nanosecond range. We have perfected an optical detector to "see" the pulses using a high speed (less than 1 ns) PIN photodiode and two 1.5 GHz bandwidth amplifiers in series. Fall times as short as 10 to 15 ns were observed. We are having some problems with the small LED power output giving low signal to noise ratios. Through possible use of high intensity laser diodes, better shielding, and impedance matching, we hope to obtain good results. Lifetimes have been measured in CdS, Si, and Ge using LED's and strobe lights. Work will begin on BAs samples in the near future with some consideration given to trapping and mobility change effects.

An analog to digital, voltage stepping, oscilloscope scanning system has been designed to scan fabricated solar cells with the light spot from the scope. Intensity modulation and time lapse photography will be used to obtain a qualitative detection of areas of abnormally high or low photoresponse. The system works well and will be limited only be the finite (large compared to a diffusion length) width of the light spot.

4. WORK PLANNED FOR THE NEXT QUARTER

4.1 FILM GROWTH

The thermodynamics and kinetics of the B_2H_6 and AsH_3 decompositions and the BAs deposition will be compared with the current experimental results and with the findings of others concerning III-V compounds. An attempt will be made to narrow the range of substrate temperature and gas flow rates to be used in future experimental film growth studies.

Substrate use to date has been largely dictated by availability of materials and the desirability for optical transmittance. Future substrate selection will be governed by the structural and thermal properties desired for polycrystalline film growth. Single crystal hexagonal zinc sulfide has been obtained and oriented for use as the next substrate material. The orientation used will be the planes perpendicular to the (0001) axis. The lattice parameter for this orientation is (3.82) within 15% of the (111) lattice parameter (3.38) of boron arsenide. This may enhance the probability of obtaining crystalline BAs. The optical transmittance of zinc sulfide will allow the optical absorption of the films to be determined on the substrate.

Investigation of alternative processes for depositing BAs will continue. It is expected that at least one of these, the synthesis from the halides (BBr_3 and $AsCl_3$) will be implemented during the next quarter.

Methods for the determination of the composition of the amorphous films will be explored.

4.2 OPTICAL AND ELECTRICAL MEASUREMENTS

Optical transmission and electrical conductivity measurements will be completed on the films grown to date and those produced during the next quarter.

The electrical measurements activity, which was initiated during the last three weeks of the first quarter will be continued on many more samples. The low temperature conductivity measurements will be used as a standard of comparison. Only selected samples will be investigated at high temperatures because of the extremely high temperatures required to drive the material "intrinsic".

Hall measurements are being initiated at the present time. The problems associated with the interpretation of the data are unknown at this point; however, the results can certainly provide a relative measure of the mobility and doping of different films.

To more specifically identify the conduction processes, V-I characteristics will be obtained with temperature as a parameter. Again, this will be performed on selected samples which show more promise than those evaluated at this time.

In the event that we manage to grow photoconductive films, the electrical characteristics under the influence of light bias will be evaluated. The effects of light bias will be used to evaluate the significance of the energy levels located within the energy gap.

☆ U.S. GOVERNMENT PRINTING OFFICE: 1980-640-258/2239